Landau-Fermi liquid analysis of the 2D t-t' Hubbard model

P. A. Frigeri[1,a], C. Honerkamp[1,2], and T. M. Rice[1]

[1] Theoretische Physik, ETH-Hönggerberg, CH-8093 Zürich, Switzerland
[2] Department of Physics, Massachusetts Institute of Technology, Cambridge MA 02139, USA [b]

February 1, 2008

Abstract. We calculate the Landau interaction function $f(\mathbf{k}, \mathbf{k}')$ for the two-dimensional t-t' Hubbard model on the square lattice using second and higher order perturbation theory. Within the Landau-Fermi liquid framework we discuss the behavior of spin and charge susceptibilities as function of the onsite interaction and band filling. In particular we analyze the role of elastic umklapp processes as driving force for the anisotropic reduction of the compressibility on parts of the Fermi surface.

PACS. 71.10.Fd Lattice fermion models (Hubbard model, etc.) – 74.72.Jt Other cuprates

1 Introduction

The Hubbard model remains one of the most studied theoretical models in the efforts to understand the high-temperature superconducting cuprates. Despite their exceptionally high transition temperatures into the superconducting state, much of the interest in these materials arises from their anomalous normal state properties over a large part of the temperature-doping phase diagram. These effects occur unequivocally and most strongly in the underdoped samples with electron densities close to half band filling where the system is a stoichiometric antiferromagnetic Mott insulator. In the underdoped regime, the transition into the superconducting state occurs out of the so-called pseudogap phase, which shows significant deviations from conventional metallic Fermi-liquid behavior[1, 2]. This is in contrast with sufficiently overdoped samples where many observations point toward a conventional transition from a Fermi-liquid into the superconducting state[3]. There have been experimental and theoretical studies suggesting that a quantum critical point hidden underneath the superconducting dome[4,5,6] or the onset of Fermi surface truncation[7,8,9] give rise to these phenomena. On the other hand one may try to take a more conservative route and attempt to understand the experimental findings within a conventional Fermi-liquid framework. Typically, rather specific assumptions on the Landau interaction function have to be made[10] in order to obtain agreement with the experimental data. Thus it appears useful to simply calculate within perturbation theory the Fermi-liquid properties of the 2D Hubbard model and to see whether these assumptions can be justified within this transparent theoretical framework.

Another motivation for this work is the question whether as the density is increased towards half filling some kind of drastic change of the low energy properties, e.g. corresponding to Fermi surface truncation as indicated by one-loop renormalization group calculations[8,9], is foreshadowed already in a perturbative Fermi liquid picture. Such a partial truncation of the Fermi surface has been argued to be seen in angular resolved photoemission experiments [7]. It is a promising candidate to understand the many anomalies of the underdoped normal state of the high-T_c cuprates, as it naturally combines insulator-like features such as the pseudogap, the observed c-axis resistivity and the strongly reduced superfluid weight, with residual metallic properties as evidenced by the in-plane transport and superconductivity itself. Since both the renormalization group approaches and the present Fermi liquid analysis are perturbative techniques, we will not obtain an accurate description of possible phases with a truncated Fermi surface, but we will carefully look for insulator-like tendencies in these calculations as the interaction gets stronger. In particular we analyze the influence of umklapp processes between $\mathbf{k}$-space regions in the vicinity of the saddle points at $(\pi, 0)$ and $(0, \pi)$. Elastic umklapp scattering with momentum transfer of (π, π) across the Fermi surface is allowed when the Fermi surface extends to the Brillouin zone boundary for a certain density range close to half filling.

A Fermi liquid analysis of the 2D Hubbard model close to half filling has been presented by Fuseya et al.[11]. These authors studied the case with only nearest neighbor hopping, t, and found a suppression of the uniform spin susceptibility for sufficiently strong interaction close to half-filling, which maybe interpreted as indicating the opening of a spin gap. Unfortunately this promising indication turns out to be an artifact of the calculation scheme used by Fuseya et al. [11], as will be discussed below. From

[a] e-mail: `pfrigeri@itp.phys.ethz.ch`
[b] present address

renormalization group studies[12,9] we know that nonzero values of the next nearest neighbor hopping, t', can change the weak coupling physics significantly. Therefore, in this paper we extend the analysis of the Landau interaction function and related quantities to the case of $t' \neq 0$. Particular attention is paid to the anisotropy of the interaction function for different parts of the Fermi surface.

In the following we first apply a second order perturbative method and discuss the **k**-space integrated and **k**-space resolved Fermi liquid properties of the 2D t-t' Hubbard model. Next we describe how ladder summations in the particle-particle and particle-hole channels, which are necessary to remove unphysical divergences, modify the tendencies observed in the second order approach. Finally we conclude and compare our results to other approaches and experimental observations for the high-T_c cuprates.

2 Second order calculation of the quasiparticle interaction

The kinetic energy for the t-t' Hubbard model on the 2D square lattice is given by

$$\epsilon_{\mathbf{k}} = -2t(\cos k_x + \cos k_y) + 4t' \cos k_x \cos k_y , \quad (1)$$

where t and t' denote the amplitudes for hopping between nearest and next-nearest neighbors, respectively. The short range Coulomb interaction between the electrons is taken into account by the usual onsite repulsion

$$H_I = U \sum_i n_{i,\uparrow} n_{i,\downarrow} . \quad (2)$$

The particle number N_e is controlled by a chemical potential μ.

The Landau interaction function $f_{s,s'}(\mathbf{k}_F, \mathbf{k}'_F)$ can be obtained [13] from the two-particle vertex $\Gamma_{ss'}(\mathbf{K}, \mathbf{K}', \mathbf{K}+\mathbf{Q})$. Here $\mathbf{K} = (\mathbf{k}, \nu)$ is a short notation for wavevectors and frequencies. Γ is a function of the interaction strength, U. To first order in U, Γ is wavevector independent, but higher orders lead to a pronounced wavevector dependence. $\mathbf{K}$, $\mathbf{K}'$ and spin indices s, s' characterize the two initial particles and $\mathbf{K}+\mathbf{Q}$, $\mathbf{K}'-\mathbf{Q}$ and s, s' their final states, and $\mathbf{Q} = (\mathbf{q}, \omega)$ denotes wavevector and frequency transfer in the scattering process. The Landau quasiparticle interaction $f(\mathbf{k}_F, \mathbf{k}'_F)$ corresponds to the vertex function in the limit $\mathbf{Q} \to 0$ with $\frac{q}{\omega} \to 0$ with $\mathbf{K} = (\mathbf{k}_F, 0)$ and $\mathbf{K}' = (\mathbf{k}'_F, 0)$. More precisely

$$f_{s,s'}(\mathbf{k}_F, \mathbf{k}'_F) = z_k z_{k'} \lim_{\omega \to 0} \lim_{\mathbf{q} \to 0} \Gamma_{s,s'}(\mathbf{K}, \mathbf{K}', \mathbf{K}+\mathbf{Q}), \quad (3)$$

where $\mathbf{k}_F$, $\mathbf{k}'_F$ are two wavevectors on the Fermi surface and z_k is the residue of the pole of the interacting one-particle Green's function $G(\mathbf{k}_F, \nu)$, i.e. $z_k = (1 - \delta \Sigma / \delta \nu)^{-1}$ with self-energy $\Sigma(\mathbf{k}, \nu)$. The two-particle vertex is determined by the coupling function $V_{ss'}(\mathbf{K}, \mathbf{K}', \mathbf{K}+\mathbf{Q}) = V(\mathbf{K}, s; \mathbf{K}', s'; \mathbf{K}+\mathbf{Q}, s)$ via

$$\begin{aligned} \Gamma_{s,s'}(\mathbf{K}, \mathbf{K}', \mathbf{K}+\mathbf{Q}) = &\delta_{s,s'}[V_{ss'}(\mathbf{K}, \mathbf{K}', \mathbf{K}+\mathbf{Q}) \\ &- V_{ss'}(\mathbf{K}', \mathbf{K}, \mathbf{K}+\mathbf{Q})] \\ &+ \delta_{s,-s'} V_{ss'}(\mathbf{K}, \mathbf{K}', \mathbf{K}+\mathbf{Q}), \quad (4) \end{aligned}$$

which expresses the fact that Γ has to be antisymmetric with respect to the exchange of two particles with the same spin orientation. Then the Landau interaction function can be obtained via (4) by taking the limit (3) in the perturbation expansion for $V_{ss'}(\mathbf{K}, \mathbf{K}', \mathbf{K}+\mathbf{Q})$. The first and second order graphs contributing are shown in Fig. 1. First the Landau function will be evaluated to second
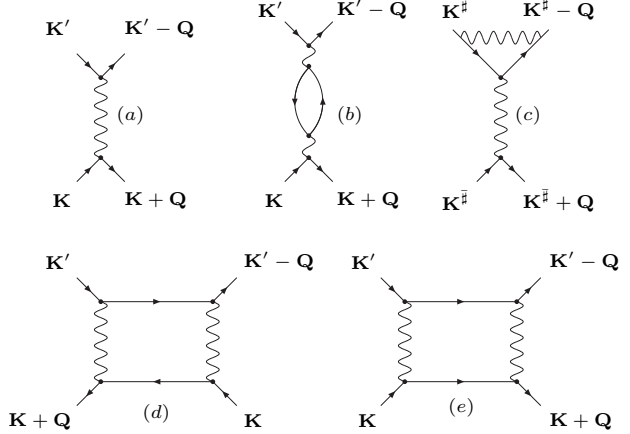

Fig. 1. First and second order graphs contributing to Γ. We use the notations $\sharp = \{ ,' \}$ and $\bar{\sharp} = \{', \}$.

order in U. Corrections from the z_k factors are at least second order in U, therefore setting $z_k = 1$ is fully consistent up to second order. The same argument justifies the neglect of effective mass corrections. Finally the second order quasiparticle interaction function reads

$$\begin{aligned} f_{\uparrow\uparrow}(\mathbf{k}_F, \mathbf{k}'_F) &= f_{\downarrow\downarrow}(\mathbf{k}_F, \mathbf{k}'_F) \\ &= U^2 \chi_{PH}(\mathbf{k}_F - \mathbf{k}'_F), \quad (5) \end{aligned}$$

$$\begin{aligned} f_{\uparrow\downarrow}(\mathbf{k}_F, \mathbf{k}'_F) &= f_{\downarrow\uparrow}(\mathbf{k}_F, \mathbf{k}'_F) \\ &= U + U^2(\chi_{PP}(\mathbf{k}_F + \mathbf{k}'_F) + \chi_{PH}(\mathbf{k}_F - \mathbf{k}'_F)), \quad (6) \end{aligned}$$

with

$$\chi_{PH}(\mathbf{q}_0) = \frac{1}{(2\pi)^2} \int d^2 p \, \frac{n_{\mathbf{p}} - n_{\mathbf{q}_0 + \mathbf{p}}}{\epsilon_{\mathbf{q}_0 + \mathbf{p}} - \epsilon_{\mathbf{p}}}. \quad (7)$$

and

$$\chi_{PP}(\mathbf{q}_0) = \frac{1}{(2\pi)^2} \int d^2 p \, \frac{1 - n_{\mathbf{p}} - n_{\mathbf{q}_0 - \mathbf{p}}}{2\mu - \epsilon_{\mathbf{p}} - \epsilon_{\mathbf{q}_0 - \mathbf{p}}}. \quad (8)$$

Here $n_p = 1/(1 + \exp(\epsilon_p - \mu)/T)$ is the Fermi distribution at temperature T.

For the analysis of the physical properties of the interacting Fermi liquid it is convenient to introduce symmetric (f^s) and antisymmetric parts (f^a) of the Landau

quasiparticle interaction by

$$f^{s,a} = \frac{1}{2}(f_{\uparrow\uparrow} \pm f_{\downarrow\uparrow}). \qquad (9)$$

$f^s(\mathbf{k}_F, \mathbf{k}'_F)$ and $f^a(\mathbf{k}_F, \mathbf{k}'_F)$ are computed for a fixed value of the chemical potential μ. $\mathbf{k}_F$ and $\mathbf{k}'_F$ are parametrized by the two angles θ and θ', measured from the symmetry axis ΓX, as shown in the inset of Fig. 5. Fig.2 shows the results obtained for the parameters $t'/t = 0.3$, $\mu/t' = -3.83$, $T/t = 0.002$ and $U/t = 1$. Note that for this choice of the chemical potential $\mu/t' > -4$, the Fermi surface consists of four arcs which lead to the breaks in the curves. The most prominent feature is the divergence along a diagonal line with $\pi < \theta' < 3\pi/2$ in both functions. This reflects simply the cooper divergence in second order perturbation theory and it is removed by summing the ladder graphs in the particle-particle channel as discussed below.
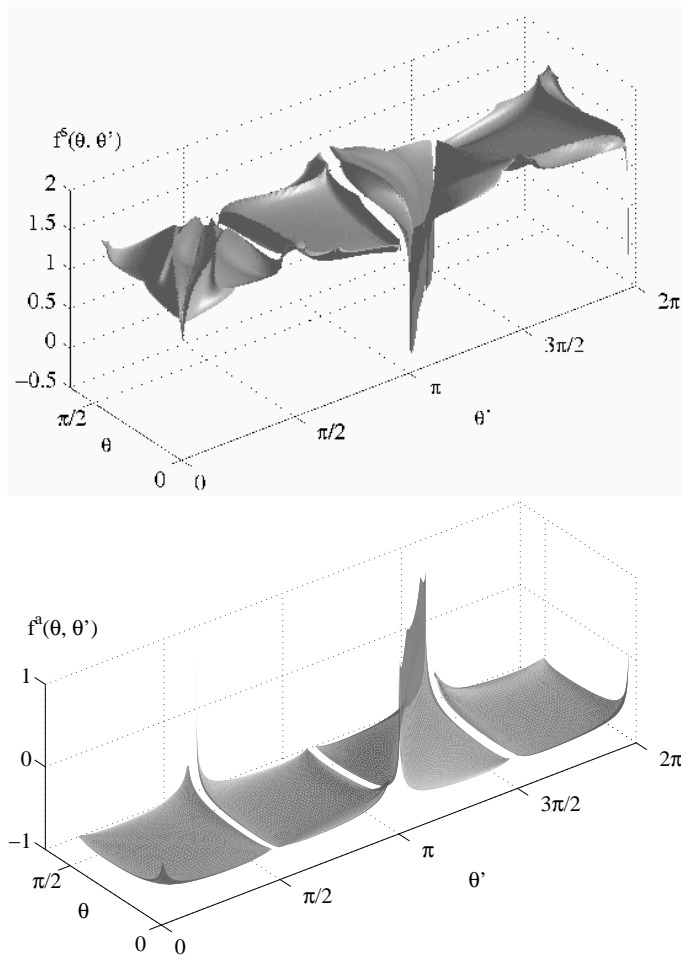

Fig. 2. Numerical results for the symmetric $f^s(\theta, \theta')$ and antisymmetric part $f^a(\theta, \theta')$ of the Landau interaction obtained by the second order perturbation approximation for the parameters $t' = 0.3t$, $\mu = -3.83t'$, $U = 1t$ and $T = 0.002t$. To the second order $f^{a,s}(\mathbf{k}_F, -\mathbf{k}_F)$ show unphysical divergences (sharp diagonal features for $\pi < \theta' < 3\pi/2$).

3 Total charge and spin susceptibility for the almost isotropic case

In a Fermi liquid the static uniform charge and spin susceptibilities X_c and X_s involve only excitations in the neighborhood of the Fermi surface. Therefore they can be calculated as Fermi surface integrals over $\mathbf{k}$-space local quantities $\chi_c(\mathbf{k}_F)$ and $\chi_s(\mathbf{k}_F)$ which define local susceptibilities for Fermi surface points described by the wavevector $\mathbf{k_F}$,

$$\rho^2 X_c = \frac{1}{\Omega}\frac{dN_e}{d\mu} = \int dl_F \, \chi_c(\mathbf{k}_F), \qquad (10)$$

$$\frac{X_s}{\mu_B^2} = \frac{1}{\mu_B^2 \Omega}\frac{dM}{dH} = \int dl_F \, \chi_s(\mathbf{k}_F). \qquad (11)$$

Here, $\int dl_F$ denotes the line integral along the Fermi surface and Ω is the total volume. N_e denotes the number of electrons and $\rho = N_e/\Omega$ denotes their density. μ_B is the Bohr magneton. The $\mathbf{k}$-space local susceptibilities are solutions of two inhomogeneous linear equations,

$$L^s(\chi_c) = 2, \qquad L^a(\chi_s) = 2, \qquad (12)$$

which express via the two linear integral operators $L^{s,a}$,

$$\frac{L^{s,a}(\chi)}{(2\pi)^2} = v_F\chi(\mathbf{k}_F) + \int \frac{dl'_F}{2\pi^2} \, f^{s,a}(\mathbf{k}_F, \mathbf{k}'_F) \, \chi(\mathbf{k}'_F), \qquad (13)$$

how the local susceptibilities are renormalized by the Landau f-function [13]. Here, $v_F \equiv v_{\mathbf{k}_F}$ denotes the magnitude of the Fermi velocity $\mathbf{v}_{\mathbf{k}_F} = \partial\epsilon_\mathbf{k}/\partial\mathbf{k}|_{\mathbf{k}=\mathbf{k}_F}$ of a quasiparticle with wavevector $\mathbf{k}$. For an isotropic Fermi surface and isotropic interactions, $\chi_c(\mathbf{k})$ and $\chi_s(\mathbf{k})$ are obviously two constants independent of $\mathbf{k}$. This allows one to express X_c and X_s using the conventional Landau parameters $F_0^{s,a}$, which are defined as zeroth order coefficients in the expansion of the Landau interaction functions $f^{s,a}$ in normalized Legendre polynomials. In the anisotropic case the Landau interaction functions can be expanded in a similar way,

$$f^{s,a}(\mathbf{k}_F, \mathbf{k}'_F) = \frac{1}{N_F}\sum_{n=0}^{\infty}\sum_{n'=0}^{\infty} F_{n,n'}^{s,a}\psi_n(\mathbf{k}_F)\psi_{n'}(\mathbf{k}'_F), \quad (14)$$

where $\psi_0(\mathbf{k}_F) = 1$, ψ_n are orthogonal functions on the Fermi surface and N_F is the density of states at the Fermi surface. Note that in general the off-diagonal terms $F_{n,n'}^{s,a} = F_{n',n}^{s,a}$ do not vanish when both ψ_n and ψ'_n belong to the same irreducible representation of the crystal symmetry group.

Initially, let us assume that the isotropic components of $f^{s,a}$,

$$F_0^{s,a} = \frac{\int\int \frac{dl_F}{v_F}\frac{dl'_F}{v'_F} f^{s,a}(\mathbf{k}_F, \mathbf{k}'_F)}{2\pi^2 \int \frac{dl_F}{v_F}} \equiv F_{0,0}^{s,a}, \qquad (15)$$

are dominant. This assumption was also made in Ref. [11]. In this case the compressibility (10) simplifies to

$$\rho^2 X_c = N_F - F_0^s \int dl'_F \chi_c(\mathbf{k}'_F)$$
$$= N_F - F_0^s \rho^2 X_c \, .$$
(16)

Thus we arrive at the well-known result for an isotropic Fermi liquid,

$$\rho^2 X_c(\mu) = \frac{N_F}{1 + F_0^s(\mu)} \, .$$
(17)

Using the same simplification we obtain for the spin susceptibility

$$\frac{X_s(\mu)}{\mu_B^2} = \frac{N_F}{1 + F_0^a(\mu)}.$$
(18)

Fuseya et al. [11] evaluated charge and spin susceptibilities for the Hubbard model with $t' = 0$ assuming that the isotropic components of $f^{s,a}$ were dominant. Their results showed a reduction of the uniform spin susceptibility for $U > 2t$ at density near to half-filling. It turns out that this effect is tied the van Hove band filling where the density of states at the Fermi surface diverges due to van Hove singularities at the saddle points $(\pi, 0)$ and $(0, \pi)$. In the special case $t' = 0$ the reduction of the spin susceptibility does not have a simple physical interpretation. In this case the van Hove filling coincides with half-filling, where the system is believed to be an antiferromagnetic insulator and the Fermi liquid approach must break down at low energy scales. But for finite next-nearest neighbor hopping $t' \neq 0$ the van Hove filling does not coincide anymore with the half-filled or perfectly nested case and in the vicinity of this filling the system may be in a paramagnetic state. In this case a reduction of the uniform spin susceptibility for $U > 2t$ could be interpreted as an indication for an opening of a spin gap in the Hubbard model close to half filling. However, our results obtained by solving the full integral equations (12), without the assumption of a dominance of the $n = 0$ terms, unfortunately remove this promising finding. This is shown in Fig. 3, where the data assuming that the isotropic terms are dominant (left panels) are compared with those obtained by solving (11, 12) (right panels). In particular in the two figures to the right the spin susceptibility does not decrease in any significant way as the van Hove filling ($\mu = 0$ for $t' = 0$ and $\mu/t' = -4$ for $t' = 0.25t$) is approached. For the charge susceptibility the qualitative behavior of the results obtained by solving (10, 12) is compatible with the one obtained by Fuseya, even if a quantitative difference is present, see Fig. 4.

Thus the conclusion of Fuseya et al.[11] that indications for a spin gap in the 2D Hubbard model can already be observed in second order perturbation theory seems to be an artifact of their approximation. The solution of the full integral equation reveals that the assumption of a dominant $l = 0$ Landau parameter is not always justified.
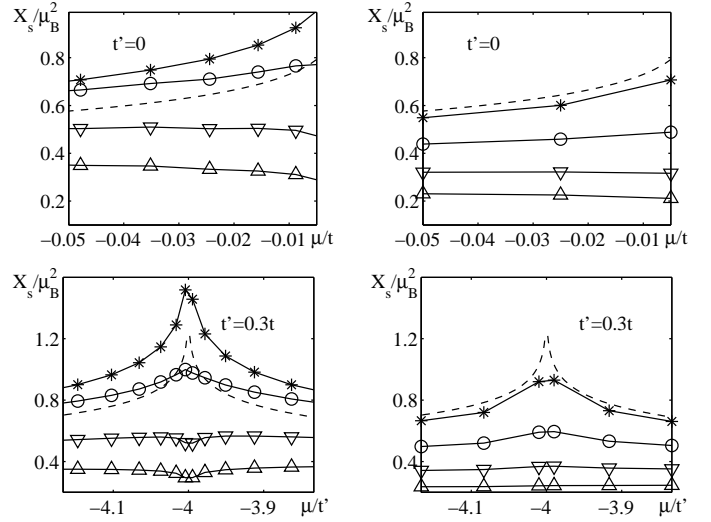

Fig. 3. Comparison between the uniform spin susceptibility X_s as function of the chemical potential μ obtained from the approximate relations (18) (plots on the left) and from the solution of the full integral equations (12,11) (plots on the right), for different values of interaction U: $*$ $U/t = 1$, $\circ$ $U/t = 2$, $\bigtriangledown$ $U/t = 3$, $\triangle$ $U/t = 4$. For all plots $T/t = 0.002$. The susceptibility for the non-interacting system ($U/t = 0$) is shown as dashed line.
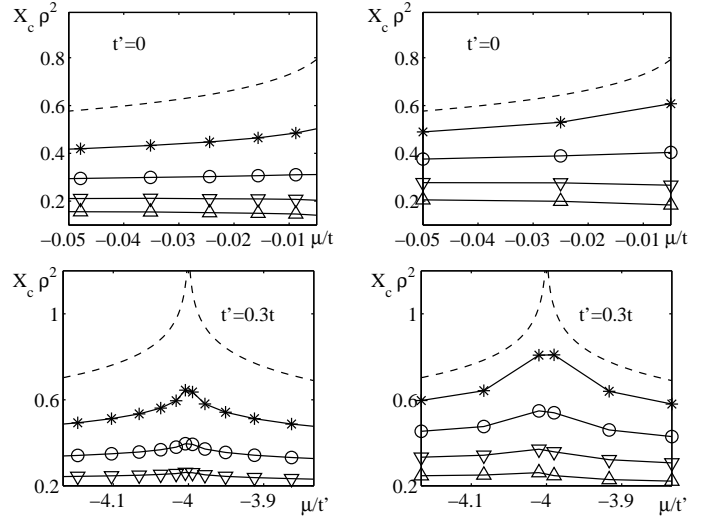

Fig. 4. Same as in Fig. 3, but for the charge susceptibility X_c.

4 Local spin and charge susceptibilities in k-space

Since the Landau interaction functions are very anisotropic, it is interesting to analyze how the local values of the static susceptibilities change with the interaction U. As mentioned in the introduction, we are particularly interested in the question whether there are tendencies towards a Fermi surface truncation, i.e. the formation of incompressible **k**-space regions at the saddle points, as suggested by one-loop renormalization group studies, already within a

low order Fermi liquid treatment. For the non-interacting system, $\chi_c(\mathbf{k}_F)$ and $\chi_s(\mathbf{k}_F)$ are proportional to the inverse velocity $1/v_{\mathbf{k}_F}$. Since $v_{\mathbf{k}_F}$ vanishes at the saddle points, a divergence appears in the local spin and charge susceptibilities around these points at the van Hove filling - a behavior opposite to incompressibility. The results for the interacting system obtained with the second order Landau function show a general reduction of the local values of the susceptibilities with increasing interaction strength U. Fig. 5 shows $\chi_s(\mathbf{k}_F)$ and $\chi_c(\mathbf{k}_F)$ when $\mathbf{k}_F$ is close to the
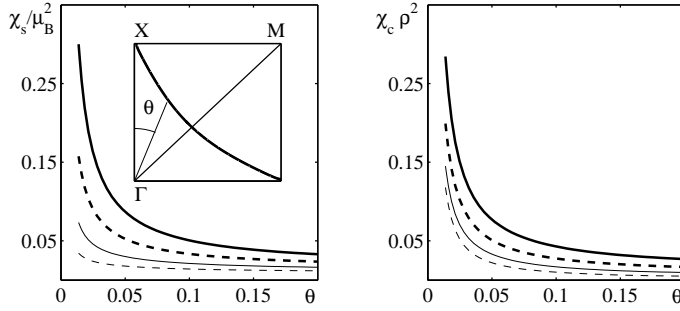

Fig. 5. k-space local values of $\chi_s(\mathbf{k}_F)$ and $\chi_c(\mathbf{k}_F)$ for $\mathbf{k}_F$ near a saddle point for different values of U: $U/t = 1$ thick line, $U/t = 2$ thick dashed line, $U/t = 3$ thin line, $U/t = 4$ thin dashed line. The inset shows how the angle θ is used to parameterize the points of the Fermi surface ($\mathbf{k}_F(\theta)$). Results computed for $t' = 0.3$, $\mu/t' = -3.99$, and $T/t = 0.002$.

saddle point. The inset in the spin susceptibility graph indicates how the angle θ is used to parameterize the points of the Fermi surface, $\mathbf{k}_F(\theta)$. Particularly interesting is the fact that near the saddle point the reduction of the local spin susceptibility is pronounced. The charge susceptibility shows a similar behavior, but in a less marked way. In
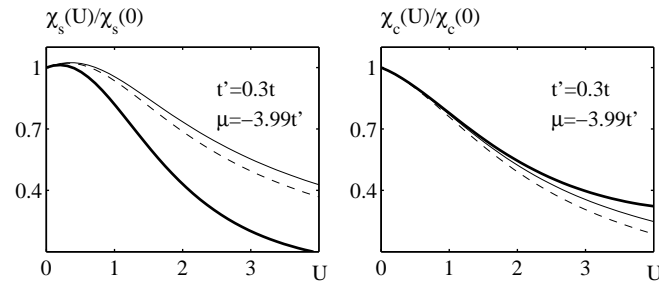

Fig. 6. Relative variations of the k-space local spin and charge susceptibilities ($\chi_s(U)$ and $\chi_c(U)$) near the van Hove filling for three different values of the angle θ as function of the interaction U. $\theta = \theta_{min}$ thick line, $\theta \approx \pi/8$ thin dashed line, $\theta = \pi/4$ thin line. $T/t = 0.002$.

fact the comparison between the two graphs of the Fig. 6 shows that the relative value of $\chi_s(\mathbf{k}_F)$ decreases more rapidly near the saddle points ($\theta = \theta_{min}$) than at other

points on the Fermi surface (e.g. $\theta \approx \pi/8$ and $\theta = \pi/4$), while for $\chi_c(\mathbf{k}_F)$ the situation is reversed.
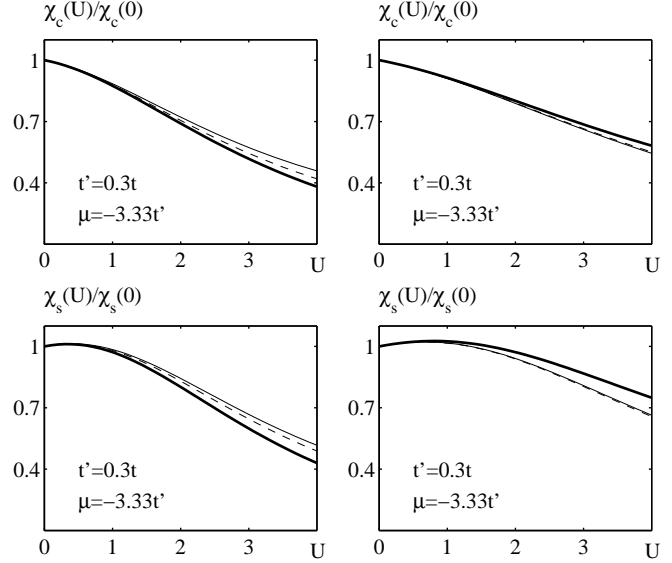

Fig. 7. Left plots: relative variation of the local spin and charge susceptibilities ($\chi_s(U)$, $\chi_c(U)$) for three different values of the angle θ as function of the interaction U. $\theta = \theta_{min}$ thick line, $\theta \approx \pi/8$ thin dashed line, $\theta = \pi/4$ thin line. $T/t = 0.002$. The band filling is larger than the van Hove filling and elastic umklapp processes at the Fermi surface are possible. Right plots: results obtained excluding all umklapp processes from the Landau interaction functions.

The behavior of the susceptibilities for values of μ further away from the van Hove filling is noteworthy, too. In particular the qualitative difference of the susceptibilities between the case $\mu > -4t'$ (density larger than van Hove filling) and $\mu < -4t'$ (density smaller than van Hove filling), deserves to be noticed. In the first case the two graphs on the left in Fig. 7 show that the relative reduction of the local susceptibilities is stronger for Fermi surface points near to XM ($\theta = \theta_{min}$), compared to Fermi surface points closer to the diagonal ΓM ($\theta \approx \pi/8$, $\theta = \pi/4$). The situation changes if the calculations are done excluding umklapp processes of all kinds from the second order contributions, see the two graphs on the right in Fig. 7. This last fact already indicates the importance of elastic umklapp scattering at the Fermi surface that is allowed for densities larger than the van Hove density. The second case is when $\mu < -4t'$ and elastic umklapp scattering does not enter the low energy physics. The two graphs on the left in Fig. 8 show a qualitative behavior of the local spin susceptibility that is similar to that observed for $\mu > -4t'$. But the strongest reduction of the local charge susceptibility is now shifted to $\theta \approx \pi/8$ and $\theta = \pi/4$ and the role of the umklapp processes becomes marginal at these densities.
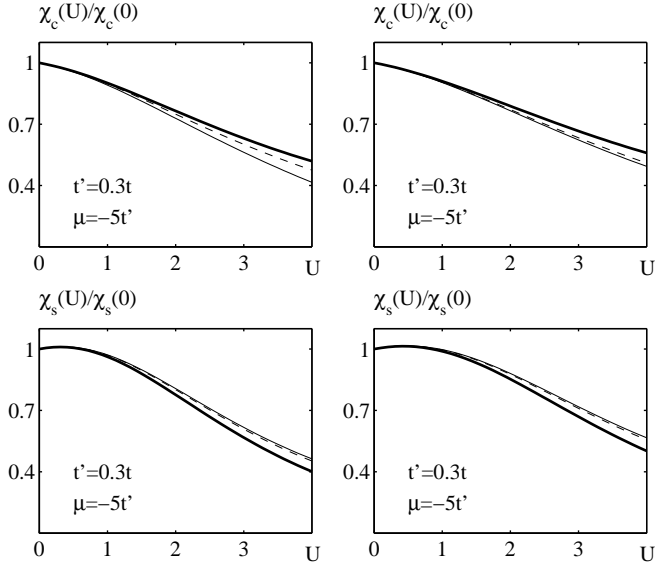
Fig. 8. Same as in Fig. 7 for band filling less than the van Hove filling such that elastic umklapp processes at the Fermi surface are absent.

5 Ladder summations

The results in the previous sections were obtained with the Landau interaction function calculated to second order in U. Although we observed a general suppression of the charge and spin susceptibility with respect to the non-interacting values, the effects were weak and no clear tendencies towards partial incompressibility could be found. In this section we extend the perturbative calculation of the Landau function to summations of infinite numbers of diagrams. Our motivation for doing this is twofold: *a)* A severe defect of the second order approach is that the contribution of the *s*-wave pairing channel to the interaction between the quasiparticles is typically overestimated to this order. In fact $f_a(\mathbf{k}_F, \mathbf{k}'_F) = -U^2 \chi_{PP}(\mathbf{k}_F + \mathbf{k}'_F)$ diverges at $T = 0$ when $\mathbf{k}'_F \to -\mathbf{k}_F$ due to the singular behavior of the Cooper graph in systems with parity $\epsilon(\mathbf{k}) = \epsilon(-\mathbf{k})$, that is clearly visible from the Fig. 2. In the following we will remedy this defect by summing up the ladder diagrams generated by the particle-particle graphs, the result is shown in the Fig. 9. In this way for $U > 0$ the net contribution of the Cooper channel at $T = 0$ will be zero. *b)* Furthermore we know that the Hubbard model close to half filling is close to an antiferromagnetic instability. This effect can be modeled in a perturbative way by summing up an infinite number of bubble and ladder diagrams in the particle-hole channel, as described below. By this we can enhance the proximity to the AF instability and simultaneously study whether the local charge and spin susceptibilities exhibit significant changes. We should add that our calculation does not aim at a quantitative determination of the phase diagram of the model. Therefore we do not worry too much about the question whether we neglect certain contributions by selecting this particular class of diagrams. Our goal is rather to include
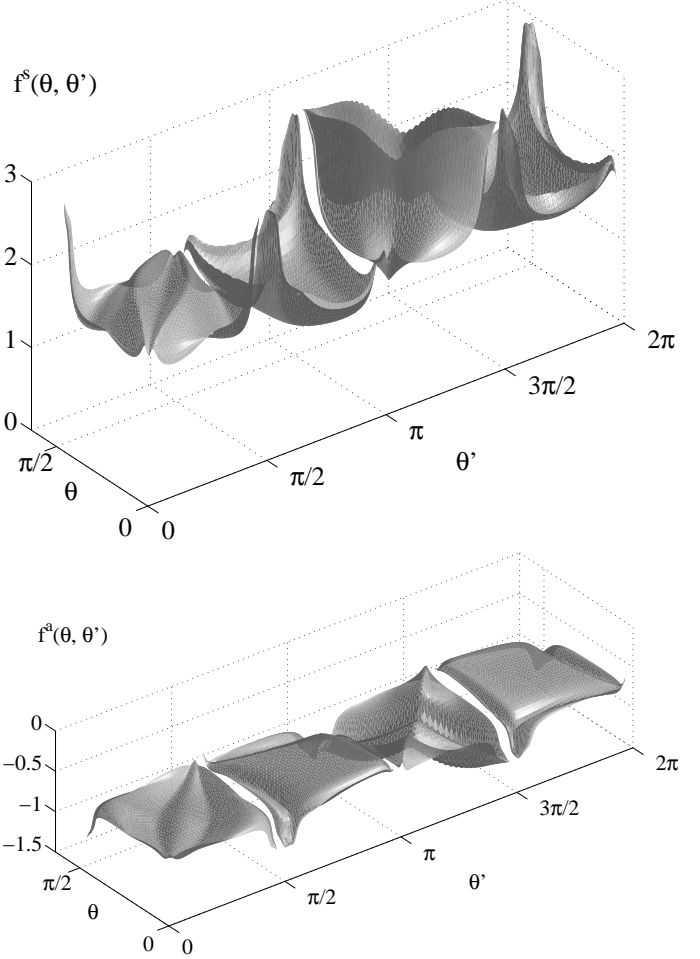

Fig. 9. Numerical solution of the symmetric $f^s(\theta, \theta')$ and antisymmetric part $f^a(\theta, \theta')$ of the Landau interaction obtained by the ladder and bubble summation for $t' = 0.3t$, $\mu = -3.83t'$, $U = 1.5t$ and $T = 0.04t$. The unphysical divergences of $f^{a,s}(\mathbf{k}_F, -\mathbf{k}_F)$ found with the second order approximation in Fig. 2 are suppressed by the ladder summation.

and enhance a specific type of scattering processes and to determine the effects of these processes on the Fermi liquid interaction and derived quantities. In the same spirit we neglect possible self energy corrections in these calculations. Within the Fermi liquid framework this concerns mainly the effective mass of the quasiparticles, but a consistent treatment should also take into account the Fermi surface shift caused by the interactions and lifetime effects on the virtual excitations in the ladder diagrams. However, since generally in spatial dimensions higher than one the self energy does not develop singularities without clear signs in the interactions and since we seek for qualitative results that do not depend on details of the model, we ignore the selfenergy effects and focus on the interaction function. This has the advantage that the analysis remains relatively simple and lucid.

The graphs contributing to the particle-particle and particle-hole ladder and bubble summations are shown in

Fig. 10. The only graph contributing to $f_{\uparrow,\uparrow}(\mathbf{k}_F, \mathbf{k}'_F)$ to the second order is the one-loop particle-hole bubble. This implies that the ladder summation for $f_{\uparrow,\uparrow}$ involves only odd powers of the bubble graph.
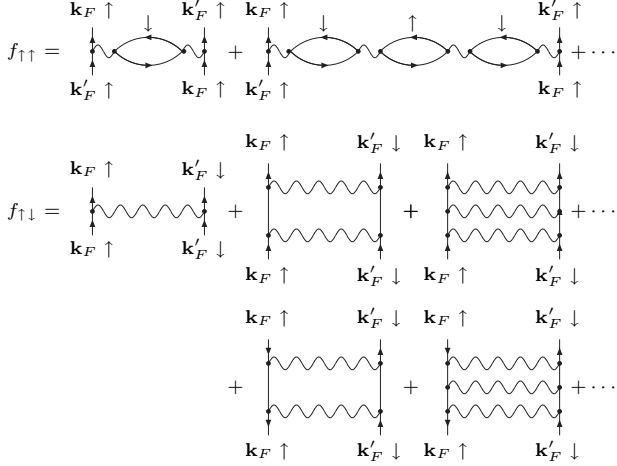

Fig. 10. Graphs contributing to the Landau interaction functions generated by the ladder summations of the first and second order graphs.

Thus the Landau interaction functions can be expressed as

$$f_{\uparrow,\uparrow} = \frac{U^2 \chi_{PH}(\mathbf{k}_F - \mathbf{k}'_F)}{1 - U^2 \chi_{PH}^2(\mathbf{k}_F - \mathbf{k}'_F)}, \tag{19}$$

$$f_{\uparrow,\downarrow} = \frac{U}{1 - U\chi_{PP}(\mathbf{k}_F + \mathbf{k}'_F)} + \frac{U^2 \chi_{PH}(\mathbf{k}_F - \mathbf{k}'_F)}{1 - U\chi_{PH}(\mathbf{k}_F - \mathbf{k}'_F)}. \tag{20}$$

With the Landau interaction function obtained above Eqns. (12) and (13) are solved again. Contrary to the second order approximation the local values of the spin susceptibility diverge to ∞ for $U > U_c$ with a critical $U_c(\mu)$ indicating a ferromagnetic instability of the system near the van Hove filling. This increased tendency towards ferromagnetism can be explained by the suppression of singlet pairing by the ladder summation. In fact the same unphysical divergence of the second order particle-particle diagram was the main reason for the suppression of the spin susceptibility in the second order results. However, a more sophisticated ladder summation using a renormalized pair scattering[14] or an renormalization group approach [9,12] will tend to suppress the spin susceptibility again. This is because singlet pairing tendencies will be generated in higher angular momentum channels, especially in the $d_{x^2-y^2}$-channel.

The behavior of the local charge susceptibility when the ladder summation is included is a consistent extension of the second order calculation with a stronger suppression of $\chi_c(\mathbf{k}_F)$ near the saddle points. The graphs on the left in Fig. 11 show $\chi_c(\mathbf{k}_F)$ with $\mathbf{k}_F$ close to a saddle point for four different values of U. At $U = 1.62t$ (thin dashed line), the local charge susceptibility goes to zero. This does not occur if the umklapp processes are excluded from the perturbation expansion, as shown in the right panel of Fig. 11. The comparison between these two last graphs confirms the fundamental role of umklapp processes for the suppression of the charge susceptibility near the saddle points. In that sense the ladder summation results for the Landau function lead to a similar behavior of the charge compressibility as the one observed in one-loop renormalization group treatments.
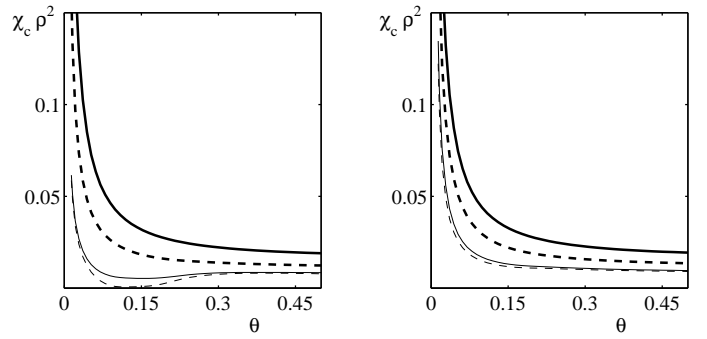

Fig. 11. Left: $\mathbf{k}$-space local values of $\chi_c(\mathbf{k}_F)$ for $\mathbf{k}_F$ near a saddle point for different values of U: $U/t = 0.5$ thick line, $U/t = 1.2$ thick dashed line, $U/t = 1.91$ thin line, $U/t = 2.05$ thin dashed line. Right: results obtained excluding umklapp processes from the perturbation expansion. For all data $t' = 0.3$, $\mu = -3.99t'$ and $T/t = 0.04$.

Another similarity with the renormalization group calculations are the tendencies towards deformations of the Fermi surface, also known as Pomeranchuk instabilities and originally suggested for the t-t' Hubbard model by Halboth and Metzner[12]. Such an instability spontaneously breaks the fourfold symmetry of the electronic dispersion. Close to the van Hove filling the main energy gain comes from lowering the kinetic energy by pushing one saddle point deeper below the Fermi level. The Landau energy functional for this process can be written, as quadratic form in the Fermi surface shifts $\delta s(\mathbf{k}_F)$,

$$\delta E = \frac{1}{(2\pi)^4} \int dl_F L^s(\delta s) \delta s(\mathbf{k}_F) \tag{21}$$

where L^s is defined by (13). Negative eigenvalues of the linear integral operator L^s imply a lowering of the energy (21) by a suitable deformation of the Fermi surface. For the specific case $t'/t = 0.3$, $\mu/t' = -3.99$ and $T/t = 0.04$ a negative eigenvalue appears already at $U/t = 1.91$, slightly before $\chi_c(\mathbf{k}_F)$ is suppressed down to zero close to the saddle points at $U/t = 2.05$. The corresponding eigenvector is shown in the graph to the left of Fig. 12 and signals a deformation $\delta s(\theta)$ of the Fermi surface breaking the point group symmetry of the square lattice, as shown schematically in the plot on the right of the same figure. No attempt

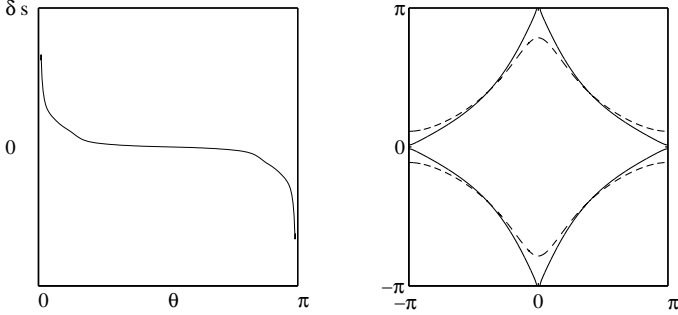was made to estimate the actual magnitude of the Fermi surface deformation.

Fig. 12. Left: unstable eigenvector $\delta s(\theta)$ of the operator $T_{\Xi_c^{-1}}$ with eigenvalue $\lambda = -0.01t < 0$ obtained for $t' = 0.3t$, $\mu = -3.99t'$, and $U/t = 1.91$. Right: Pomeranchuk deformation of the Fermi surface $\propto \mathbf{v}(\theta)\delta s(\theta)$.

In the case $t' = 0.3t$, the above scenario is observed for a very large range of chemical potential values, i.e. between $\mu/t' = -5.66$ and $\mu/t' = -3.33$. Note however that this instability is only one example out of many potential instabilities of the 2D Hubbard model close to half filling. A direct comparison of several types of instabilities can be found in Ref. [15].

6 Current carried by the quasiparticle and the Drude weight

According to Landau-Fermi liquid theory the current $\mathbf{J}_{\mathbf{k}_F}$ carried by the quasiparticle $\mathbf{k}_F$ is given by[13]

$$\mathbf{J}_{\mathbf{k}_F} = \mathbf{v}_{\mathbf{k}_F} + \int \frac{dl'_F}{4\pi^2 v'_F} \, f^s(\mathbf{k}_F, \mathbf{k}'_F) \, \mathbf{v}_{\mathbf{k}'_F}. \qquad (22)$$

The first term of (22) describes the current of the bare quasiparticle and the second one the "backflow" of the medium around it. The Drude weight is connected to the quasiparticle current via [13]

$$D^{\alpha\beta} = \pi e^2 \int \frac{dl_F}{4\pi^2 v_F} \, v_{\mathbf{k}_F}^\alpha J_{\mathbf{k}_F}^\beta. \qquad (23)$$

With a simple symmetry argument it is easy to show that the off-diagonal components vanish. This remains true even when a Pomeranchuk instability breaks the point group symmetry of the square lattice, inducing a tetragonal symmetry. The Pomeranchuk instability merely modifies the diagonal elements D^{aa} and D^{bb}, which would take different values. In this section we will assume that no Pomeranchuk instability affects the system, so that $D^{aa}=D^{bb}=D$.

Note that in a Galilean invariant system the total current is a constant of motion and does not change when the interaction is switched on adiabatically. But as a lattice model the Hubbard model does not belong to this

class of systems, thus the magnitude of D is related to the strength of the interaction U. Fig. 13 shows the change of the Drude weight when the Landau interaction function that is used to solve (22) and (23) is approximated by the ladder and bubble summations (19) and (20). The thick lines show $D(U)/(e^2\pi)$ for three different values of the chemical potential μ. With increasing interaction U, the Drude weight is reduced and goes to zero for a finite U. The reduction occurs for smaller interactions the closer the electron density is to the van Hove filling. We
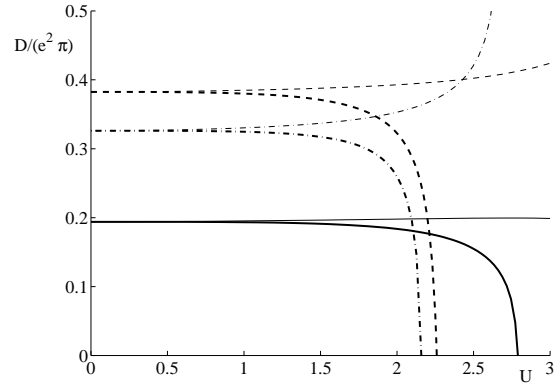

Fig. 13. The thick lines show $D(U)$ obtained by the ladder summation for three different values of μ: $\mu/t' = -3.33$ dashed line, $\mu/t' = -3.99$ dash-dotted line, $\mu/t' = -5.66$ continuous line and T=0.04t. The thin lines show the corresponding results obtained excluding the umklapp process.

note that in our calculation the Drude weight vanishes only at interaction strengths that are larger than the critical value necessary to induce the Pomeranchuk instability (U_p: $U/t = 2.075$ for $\mu = -3.33t$, $U/t = 1.91$ for $\mu = -3.99t$ and $U/t = 2.6$ for $\mu = -5.66t$). Thus the above results have no clear physical meaning for $U > U_p$. The behavior of the Drude weight for $U < U_p$, however, provides some useful information: as shown in Fig. 13, its decrease is strongest at the van Hove filling, $\mu = -4t'$. In addition, the results confirm again the important role played by the umklapp processes. In fact, if they are excluded from the calculation (thin lines of the Fig. 13), the magnitude of the Drude weight even increases with the strength of U.

It is interesting to determine the scattering processes responsible for the decrease of D. The continuous lines plotted in Fig. 14 show the symmetric Landau interaction function $f(\theta, \theta')$ for $\mu/t' = -3.33$ that has been used to solve (22) for different values of θ and as function of θ'. The thick vertical lines mark the different values of θ and the thin lines are plotted to emphasize the relevant peaks of $f(\theta, \theta')$ for the given θ. The insets shows the locations of $\mathbf{k}_F(\theta)$ (thick line) and $\mathbf{k}'_F(\theta')$ (thin lines) where the peaks in $f(\theta, \theta')$ occur.

Fig.14 shows that the peaks in the Landau function for fillings larger than the van Hove filling are tied to the Fermi surface points $\mathbf{k}_F$, $\mathbf{k}'_F$ which can be connected by
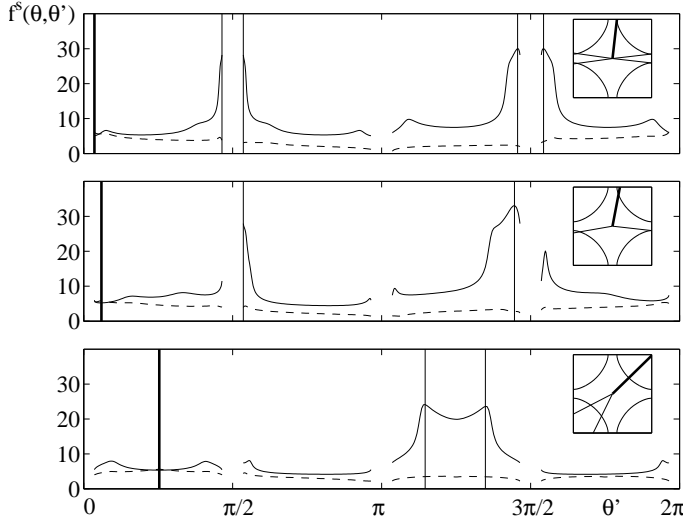
Fig. 14. The continuous lines show $f(\theta, \theta')$ for $\mu/t' = -3.33$, $U = 2.075t$ and $T = 0.04t$, obtained for three different values of θ, as a function of θ'. The thick vertical lines mark the different values of θ and the thin vertical ones are plotted to emphasize the relevant peaks of $f(\theta, \theta')$. The insets show the locations of the Fermi surface points marked by the thick and thin lines. The dashed lines show the corresponding results of $f(\theta, \theta')$ obtained excluding the umklapp process.

wavevectors close to (π, π), i.e. $\mathbf{q}_0 = \mathbf{k}_F - \mathbf{k}'_F \simeq (\pm\pi, \pm\pi)$. These processes are enhanced in the ladder and bubble summation of the terms involving $\chi_{PH}(\mathbf{q}_0)$ (7). For fillings smaller than the van Hove filling and $-6.6 < \mu/t' < -4$ the Fermi surface is partially nested and the peaks appear when $\mathbf{q}_0 = \mathbf{k}_F - \mathbf{k}'_F$ is equal to the corresponding nesting vectors (that are smaller than (π, π)). For $\mu/t' < -6.6$ the Fermi surface is strictly convex and the Drude weight increases with the strength of U.

Without umklapp processes the relevant peaks of f^s disappear, the corresponding Landau interaction (thin dashed lines of the Fig. 14) causes a "backflow" of the medium in the direction of the bare quasiparticle current implying the increase of $\mathbf{J}_{\mathbf{k}_F}$ for anyvalue of $\mathbf{k}_F$. Thus the Drude weight will increase.

7 Conclusions

We have presented a detailed study of the Landau interaction function $f(\mathbf{k}, \mathbf{k}')$ and wave-vector resolved compressibilities within Fermi liquid theory for the two-dimensional Hubbard model. This model is often considered as minimal model for the description of high-T_c superconductivity in the copper-oxide materials.

A less surprising conclusion of this work is that a Fermi liquid picture alone can hardly account for the observed anomalies that occur in the underdoped high-T_c materials when the doping is reduced towards half-filling: all effects are rather weak and one has to resort to stronger interactions U or move closer to a magnetic instability (e.g.

by ladder summations) to obtain sizable effects such as a significant reduction of the compressibility on parts of the Fermi surface. No rapid decrease of the spin susceptibility reminiscent of spin gap formation[11] can be found. Similar conclusions regarding the high-T_c cuprates were reached by Kim and Coffey[16] who analyzed the spectral function of the 2D Hubbard model within random phase approximation.

On the other hand, our weak coupling analysis provides insights into the physical processes which lead to deviations from the conventional picture. We find that many of the observed tendencies towards partially insulating behavior - as we believe an essential ingredient of the underdoped cuprate superconductors - are related to elastic umklapp processes. These processes start to affect the low energy physics upon reducing the doping when the Fermi surface touches the Brillouin zone boundaries. As we know from earlier renormalization group studies[8,9] of the same model, strong umklapp processes with momentum transfer (π, π) between the saddle point regions lead to an interesting mutual reinforcement of antiferromagnetic and d-wave pairing correlations. Furthermore the renormalization group treatment yielded a regime with a strong suppression of the charge compressibility near the saddle points. A similar effect was observed by Otsuka et al.[17] in quantum Monte Carlo calculations for $U = 4t$. In our Fermi liquid analysis we clearly identify the elastic umklapp processes as being responsible for a strong reduction of the Drude weight and the angle resolved charge compressibility on parts of the Fermi surface. In one-dimensional systems it is well known that elastic umklapp processes imply these effects. Our calculations shows that in the 2D Hubbard model there are observable tendencies in the same direction. Although our perturbative analysis does not allow to conclude that umklapp processes are the ultimate cause for the pseudogap features at stronger interactions, they will at least contribute to a certain extent. Furthermore there is no obvious reason why the importance of the umklapp scattering should decrease again for stronger interactions.

Our perturbative calculations show tendencies which can be interpreted as precursors to stronger reductions in the compressibility and Drude weight at stronger interactions, features which appear in some phenomenological descriptions of the socalled pseudogap region of the phase diagram of the underdoped cuprates. In this way they support the proposal that the critical doping of the cuprates that separates the underdoped and overdoped regimes [4], is determined by the appearance of elastic umklapp scattering with momentum transfer (π, π) connecting the Fermi surface regions near to the saddle points.

References

1. P.W. Anderson, *The Theory of Superconductivity in the High-T_c Cuprates*, Princeton University Press (1997).
2. T. Timusk and B. Statt, Rep.Prog.Phys. **62**, 61 (1999).
3. C. Proust, E. Boaknin, R.W. Hill, L. Taillefer, and A.P. Mackenzie, cond-mat/0202101.
4. J.L. Tallon and J.W. Loram, Physica C **349**, 53 (2001).
5. M. Vojta, Y. Zhang, and S. Sachdev, Phys. Rev. B**62**, 6721 (2000).
6. S. Chakravarty, R.B. Laughlin, D.K. Morr, and C. Nayak, Phys. Rev. B **63**, 094503; S. Chakravarty, Hae-Young Kee, and C. Nayak, Int. J. Mod. Phys. B **15**, 2901 (2001).
7. M.R.Norman et al., Nature **392**, 157 (1998).
8. N. Furukawa, T.M. Rice, and M. Salmhofer, Phys.Rev.Lett. **81**, 3195 (1998).
9. C.Honerkamp, M.Salmhofer, N.Furukawa, and T.M. Rice, Phys. Rev. B **63** 35109 (2001); C. Honerkamp, Euro. Phys. J. B **21**, 81 (2001).
10. A.J. Millis, S.M. Girvin, L.B. Ioffe, A.I. Larkin, J. Phys. Chem. Sol. **59**, 1742 (1998).
11. Y. Fuseya, H. Maebashi, S. Yotsuhashi and Kazumasa Miyake, J. Phys. Soc. of Japan Vol. **69** 2158 (2000).
12. C.J. Halboth and W. Metzner, Phys. Rev. B **61**, 7364 (2000); Phys. Rev. Lett. **85**, 5162 (2000).
13. Philippe Nozieres: Theory of Interacting Fermi Systems, Advanced book classics ('97).
14. D.J. Scalapino, E. Loh Jr., and J.E. Hirsch, Phys. Rev. B**35** 6694 (1987).
15. C. Honerkamp, M. Salmhofer, and T.M. Rice, submitted to EPJB.
16. J. Kim and D. Coffey, Phys. Rev. B**62**, 4288 (2000).
17. Y. Otsuka, Y. Morita, Y. Hatsugai, cond-mat/0106420.